# Enhanced comprehensive performance of bonding interface between CFRP and steel by a novel film adhesive

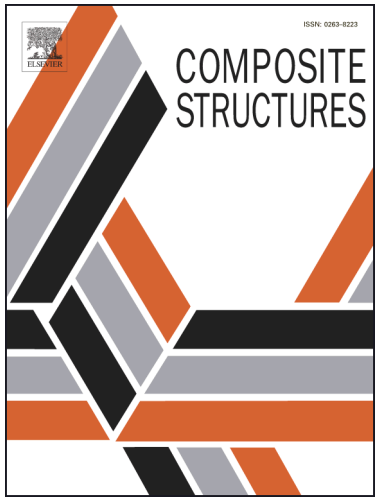


# Enhanced comprehensive performance of bonding interface between CFRP and steel by a novel film adhesive

Lu Ke, Chuanxi Li, Nanhai Luo, Jun He, Yang Jiao, Yongming Liu

PII: S0263-8223(19)32081-1
DOI: https://doi.org/10.1016/j.compstruct.2019.111393
Reference: COST 111393

To appear in: *Composite Structures*

Received Date: 2 June 2019
Revised Date: 4 August 2019
Accepted Date: 9 September 2019

Please cite this article as: Ke, L., Li, C., Luo, N., He, J., Jiao, Y., Liu, Y., Enhanced comprehensive performance of bonding interface between CFRP and steel by a novel film adhesive, *Composite Structures* (2019), doi: https://doi.org/10.1016/j.compstruct.2019.111393

# Enhanced comprehensive performance of bonding interface between CFRP and steel by a novel film adhesive

Lu Ke [a,b,c], Chuanxi Li [a,b,*], Nanhai Luo [b], Jun He [b,d], Yang Jiao [c], Yongming Liu [e]

a. Key Laboratory of Bridge Engineering Safety Control by Department of Education, Changsha University of Science and Technology, Changsha 410114, China
b. School of Civil Engineering, Changsha University of Science and Technology, Changsha 410114, China
c. Materials Science and Engineering, Arizona State University, Tempe, AZ 85287, USA
d. Institute for Infrastructure and Environment, Heriot-Watt University, Edinburgh, Currie EH14 4AS, UK
e. Aerospace and mechanical engineering, Arizona State University, Tempe, AZ 85287, USA

## Abstract:

A novel film adhesive was proposed to bond carbon fiber reinforced polymer (CFRP) laminas to steel substrates, and experimental validations for improved comprehensive bond performances are presented. This film adhesive was shown to possess excellent high-temperature resistance via dynamic mechanical analysis (DMA). A series of CFRP/steel double-lap joints (DLJs) with different bond lengths were experimentally studied, focusing on the failure modes, effective bond length, bond-slip relationship, and bond strength. The results show that the film-adhesive bonded joints fail in the mode of CFRP delamination, which indicates a stronger interfacial bond between the adhesive layer and adherends than the intra-laminar strength of CFRPs. The bonding interface has an effective bond length of approximately 65 mm, beyond which no increase of ultimate load can be achieved with the increase of bond length. The bond-slip relationship of the film-adhesive bonding interface exhibits a trapezoidal (ductile) shape, which is significantly different from the triangular (brittle) shapes for most paste-adhesive interfaces. Superior strength, ductility, and high-temperature resistance of the bonding interfaces in CFRP/steel composites are achieved due to the use of this film adhesive. The proposed study offers an alternative solution to an enhanced comprehensive property of the bonding interface in CFRP/steel composites.

## Keywords:

Bond performance; carbon fiber reinforced polymer (CFRP); steel; film adhesive; bond-slip relationship

*Corresponding author at: School of Civil Engineering, Changsha University of Science & Technology, Changsha 410114, China.

E-mail addresses: clkelu@foxmail.com (L. Ke), lichuanxi2@163.com (C. Li)

## Highlights:

1. A novel film adhesive was first proposed for bonding CFRP laminas to steel substrates.
2. Effective bond length and bond-slip relationships for the film-adhesive bonding interfaces are established.
3. Behaviors of the film-adhesive bonding interface are systematically compared with traditional paste-adhesive ones.
4. Excellent comprehensive bond performance of CFRP/steel composite is achieved by the film adhesive.

## 1. Introduction

Carbon fiber reinforced polymer (CFRP) has shown a great application potential for the maintenance of civil infrastructures due to its high specific strength and stiffness, good fatigue resistance, and excellent environmental durability [1,2]. Compared with its application in the strengthening of concrete structures [3-6], the application of CFRP in the strengthening of steel structures, however, is still immature and challenging [1,7-10]. The bonding interface between CFRP and steel often exhibits as the weakest link and constitutes one of the central issues affecting the behavior of CFRP-strengthened steel structures [11-19]. As demonstrated by the previous studies on the CFRP/steel bonding interfaces with paste epoxy adhesives, the bond behavior, including the failure mode, bond-slip relationship, and bond strength, heavily depends on the material properties of adhesive [12,20-22]. Consequently, the selection of a suitable adhesive is vital for the application of CFRP/steel bonded composites and requests the engineers have a thorough understanding of not only the material characters of adhesive but also the interfacial behavior within composites.

Most existing studies on the CFRP/steel bond have focused on the bond strength, rather than the comprehensive consideration of bond strength and toughness in a progressive fashion. The failure mode of CFRP/steel bonded composites is closely related to the interfacial bond-slip constitutive relationship, which is critical for the understanding and modeling of interfacial behaviors, e.g., the bond strength and toughness [11,12,20]. The failure of CFRP/steel composites often manifests in forms of (a) CFRP-adhesive interface debonding, (b) steel-adhesive interface debonding, (c) cohesive failure, (d) CFRP delamination, (e) CFRP fracture, etc. [1,11,12,20]. In previous studies, most paste-adhesive bonded joints had interfacial debonding failures such as modes a, b, and c or their mixed modes [11,12,16,20,23-26]. These interfacial debonding failures often show brittle characteristics, and their presence implies that the material properties of adhesive have not been fully utilized. Cohesive failure (mode c) has ever been recommended as a proper failure pattern [27]. However, recent researches showed that bonding interfaces with cohesive failure might have either bilinear (brittle) or trapezoidal (ductile) bond-slip relationship, which depends on how ductile the adhesive is [12,26,28,29]. In contrast, the CFRP delamination (mode d) definitely shows characteristics of ductile fracture because a plateau segment is observed in its interfacial bond-slip curve [12,28,30].

In fact, the CFRP material and CFRP/steel bonded composite structures typically behave in more or less a brittle manner compared with CFRP/concrete or CFRP/timber composites [31,32]. In order to compensate for the lacking ductility, especially in the case of dynamic loading conditions, ductility can be incorporated in the structural system, e.g., by adopting a ductile adhesive layer. Indeed, the use of a ductile adhesive layer is conducive to an appropriate failure mode of CFRP/steel composites –cohesive failure or CFRP delamination [29,32]. Moreover, as revealed in previous studies, the bond strength between CFRP and steel is closely related to the interfacial fracture energy which relies on both the ductility and tensile strength of adhesives [9,12,20,29]. Thus, the use of a ductile adhesive contributes to not only the interfacial ductility but also the bond strength [29,33,34]. However, studies involving the failure mechanisms of ductile bonding interfaces are very limited.

On the other hand, the high-temperature service environment is a bad condition that is needed to be considered in the application of epoxy adhesives in civil infrastructures. It is because that it's normal for infrastructures in many regions worldwide to be subjected to elevated temperatures of 50-70°C, which the mechanical behaviors of epoxy adhesives are often sensitive to [22,35-37]. In fact, the effects of elevated temperatures on the bond behavior in CFRP/steel composites have

been proved significant in existing researches [8,22,36-38]. Consequently, other than the bond strength, considerations for the ductility and high-temperature resistance of the bonding interface are needed to be integrated into the investigations.

In this paper, an innovative ductile film adhesive was employed to bond CFRP laminas to steel substrates. The film adhesive, which is supported with nylon-fabric carrier, was evidenced to possess excellent high-temperature resistance via dynamic mechanical analysis (DMA). The objective of the paper is to investigate the effectiveness of the new film adhesive for bonding CFRP to steel structures regarding the strength, ductility and high-temperature resistance. A series of CFRP/steel double-lap joints (DLJs) with different bond lengths were fabricated with this film adhesive and tested in a tension set-up. First, experimental results including failure mode, load-displacement response, strain distributions on the surface of CFRP, and bond stress distributions within the bonding interface were presented. After that, the bond-slip relationships of the film-adhesive bonding interface were established based on the above test results and compared with those of traditional paste-adhesive bond lines. At last, the bond strengths of the film-adhesive joints with a sufficient bond length are compared with those of paste-adhesive joints, and the frequently used analytical model for the bond strength was validated with both the experimental and collected data. This research provides a novel solution for bonding CFRP laminas to steel structures as a composite or retrofitting program.

## 2. Experimental program

### 2.1. Materials

The unidirectional CFRP plates used in this study were fabricated by pultrusion forming techniques in Nanjing Hitech Co., Ltd., and the steel plates used are bridge structural steel Q345qD. A nylon-fabric carrier supported epoxy film adhesive J-69E was utilized as the bonding material. This film adhesive is developed by a China research institute and has been applied in some subway and high-speed trains, and curtain walls of buildings. The photographs of the film adhesive and nylon- fabric carrier within the film adhesive are presented in Fig. 1. The nylon-fabric carrier is of mesh size of 2.5mm. The film adhesive is modified with engineering plastic and core-shell structured nanoparticles to enhance the mechanical resistance against elevated temperatures. It needs to be cured at 90 °C–120 °C for about 2h to active the curing agent. A unique advantage for the film adhesive is that latent curing agent dicyandiamide and the nylon-fabric carrier are applied in the adhesive, which makes the adhesive a solid film and brings great conveniences for the storage and conveyance of the adhesive materials. More significantly, the nylon-fabric carrier also makes the control of adhesive layer thickness easy during the curing process, especially when used for the repair of structures with complex configurations.

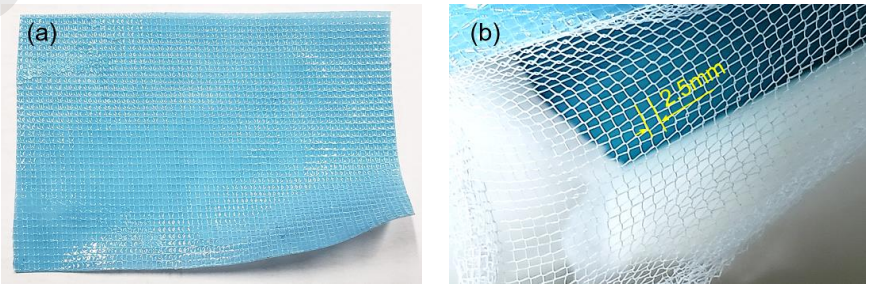


**Fig. 1 Photographs of (a) film adhesive and (b) nylon-fabric carrier within the film adhesive.**

The dog-bone-shape specimens were fabricated using the adhesive matrix without the nylon-fabric carrier according to ASTM D638-14 [39], and the tensile engineering stress-strain

relationship for the film adhesive was obtained, as shown in Fig. 2. As shown in this figure, the tensile stress almost increases linearly with the strain when the strain is less than 1%. However, the stress rises nonlinearly with the increasing strain when the strain exceeds 1%. Another notable feature for the stress-strain constitutive relationship is the relatively large strain at break, which also shows the superior ductility of the adhesive. The material properties of the CFRP, steel plate, and film adhesive are listed in Table 1. The material properties of the CFRP and the shear strengths for film-adhesive joints were provided by the manufacturers. The tensile properties of the steel plate and the adhesive were obtained from tensile tests of tensile specimens.

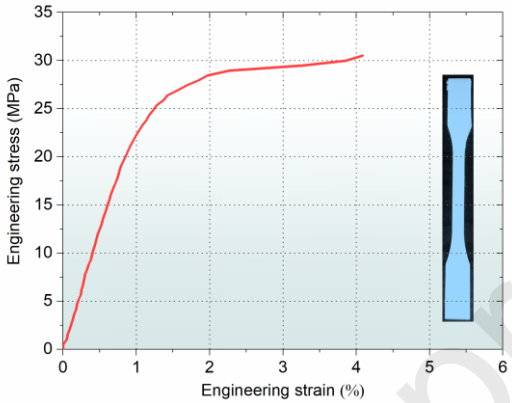


**Fig. 2 Engineering stress-strain relationship for the matrix of film adhesive**

**Table 1 Material properties of CFRP laminate, steel plate and film adhesive.**

| Material parameter | CFRP lamina | Steel plate | Film adhesive |
|---|---|---|---|
| Thickness (mm) | 1.4 | 12 | 0.30 ±0.02 |
| Width (mm) | 50 | 50 | – |
| Tensile strength (MPa) | 2263 | 461* | 30.50** |
| Elasticity modulus (GPa) | 161.2 | 200 | 2.39** |
| Elongation at break (%) | 1.65 | – | 4.12** |
| Shear strength for aluminum-to-aluminum joints (MPa) | – | – | 28.53 |
| Shear strength for steel-to-steel joints (MPa) | – | – | 33.30 |

* yield strength, ** tensile properties of the adhesive matrix without nylon-fabric carrier.

### 2.2. Specimen preparation

In this study, a total of 15 CFRP/steel DLJs were fabricated using the new film adhesive as per the ASTM standard D3528-96 (2016) [40]. Different bond lengths (50 /80 /120 /160 /200 mm) were selected to investigate the effective bond length of the joint specimens because the effective bond lengths for paste adhesive joints are 85–110 mm according to previous studies [18,23,41]. Taking the specimens with a bond length 200 mm as an example, we illustrated the schematic drawing of the DLJs and the strain gauges arrangement, as shown in Fig. 3. The strain gauges were numbered in sequence from the loaded end to the free end. Strain gauges with larger label numbers (close to the free end) were canceled for the specimens with shorter bond lengths. The specimens were divided into five series (Series I–V), with three same samples in each series. The parameters of the specimens are listed in Table 2.

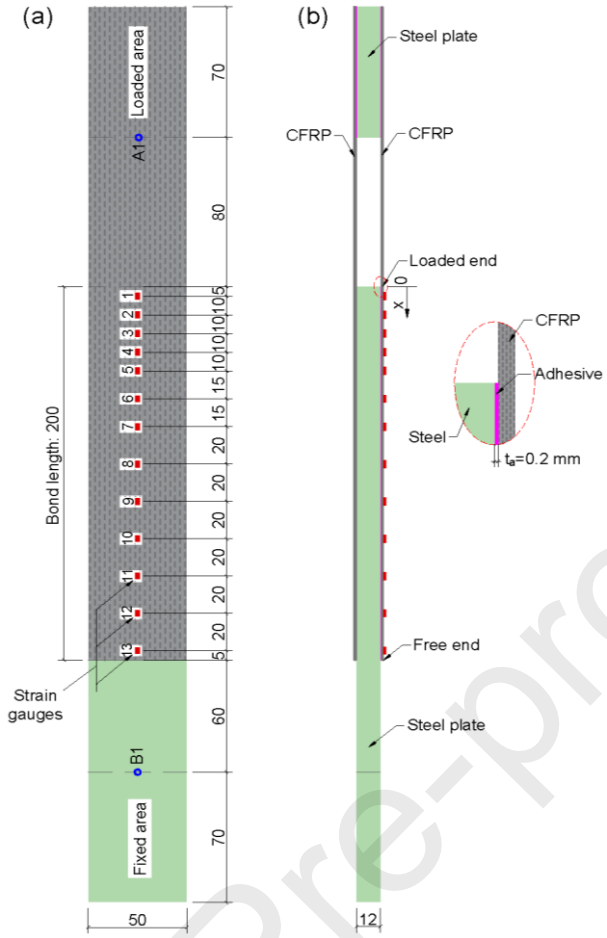


**Fig. 3 Schematic drawing of DLJ specimens and strain gauges arrangement (unit: mm): (a) plan view; (b) side view.**

**Table 2 Overview of the parameters of DLJ specimens.**

| Series | Number of specimens | Bond length (mm) | CFRP thickness (mm) | Steel plate thickness (mm) | Measured adhesive layer thickness (mm) |
|---|---|---|---|---|---|
| Ⅰ | 3 | 50 | 1.4 | 12 | 0.19 ±0.02 |
| Ⅱ | 3 | 80 | 1.4 | 12 | 0.20 ±0.02 |
| Ⅲ | 3 | 120 | 1.4 | 12 | 0.19 ±0.03 |
| Ⅳ | 3 | 160 | 1.4 | 12 | 0.20 ±0.04 |
| Ⅴ | 3 | 200 | 1.4 | 12 | 0.21 ±0.04 |

Firstly, the steel plates were ground using a grinding machine to obtain an identical surface morphology. The CFRP laminas were proceeded by sandpapers for the removal of release agent that remains on the surface during the material fabrication. The surfaces of steel and CFRP plates were then cleaned with acetone to get rid of dirt, rust, and residues prior to the application of adhesives. Secondly, the CFRPs were bonded to the steel with the film adhesive. Finally, the specimens were cured at 90°C for 2h in a temperature chamber, with steel blocks being uniformly distributed on the CFRPs to maintain a pressure of about 0.05 MPa within the bond lines.

For the convenience of description, the adhesive layer close to the loaded and fixed areas are respectively denoted as “loaded end” and “free end”, as illustrated in Fig. 3(b). A coordinate system is also defined along the direction of bond length. In the tests, the strains of CFRPs are captured by the strain gauges attached to the top surfaces of CFRP along the length direction. The strain gauges are numbered in sequence along the direction of the coordinate system, as shown in Fig. 3(a).

### 2.3. Test methods

#### 2.3.1. Dynamic mechanical analysis (DMA) of adhesives

Dynamic mechanical analysis (DMA), via depicting the storage modulus, loss modulus, and loss factor (damping) as a function of temperatures, characterizes the temperature dependency of intrinsic mechanical properties for viscoelastic materials. The loss factor $\tan\delta$ is defined as the ratio of loss modulus to storage modulus. The glass transition temperature (GTT) is often defined using the storage modulus or loss factor curves to represent the temperature dependency of adhesive storage modulus. As revealed in previous studies, the bond-slip behavior of bonded joints closely relates to the GTT of the adhesive [38,42,43]. Concretely, there exists a good correlation between the normalized temperature-dependent joint strength and adhesive storage modulus [38]. Thus, the degradation of bonded joint mechanical properties can be, to some extent, reflected by the GTT of adhesives.

Before the DMA tests, the film adhesive was cured at 90℃ for 2h, with the same curing condition as the DLJ specimens. The DMA tests for the film adhesive were performed via the application of an oscillatory tension strain to the specimens using dynamic mechanical analyzer TA DMA Q800, at a fixed frequency of 1 Hz. In the test, the investigated temperature range was 0-120℃, and the temperature ramp rate was set as 2℃/min.

#### 2.3.2. Tension-shear tests of bonded joints

The tension-shear tests for the bonded joints were carried out on an MTS landmark 810 test machine with a load capacity of 25t. Prior to the test, the specimens should be strictly aligned with the hydraulic fixtures to avoid bending moment on the specimens caused by improper centering error. At a room environment (about 25℃, relative humidity 65%), the experiments were conducted under a displacement control mode, at a loading rate of 0.4 mm/min. Strain data were collected using a TDS150 static data acquisition system. The experimental set-up for the DLJs is shown in Fig. 4.

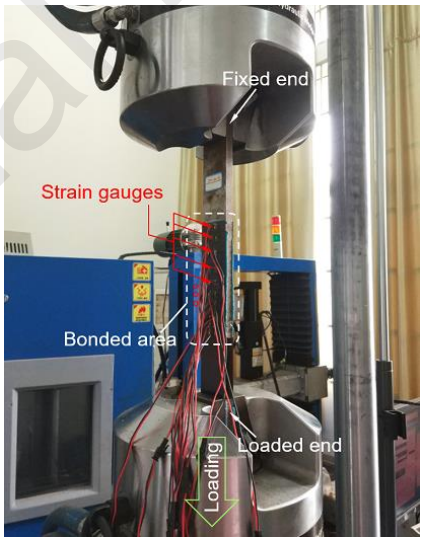


**Fig. 4 Experimental set-up for DLJ specimens.**

## 3. Experimental Results

### 3.1. Dynamic mechanical analysis (DMA)

#### 3.1.1. Dynamic mechanical behavior of film adhesives

The molecular bonds within polymer materials can be mainly divided into two categories.

The first type of bonds is the covalent intra-molecular bond which composes the principal link and skeleton of polymer chains. The second category of bonds consists of several types of secondary inter-molecular bonds such as hydrogen bond, dipole, and Van der Waals interactions [44]. The DMA results for the film adhesive J-69E are illustrated in Fig. 5, including the storage modulus, loss modulus and loss factor of film adhesive as a function of temperature. The results demonstrate that the mechanical response of the epoxy film adhesive exhibits three distinct phases as the temperature increases. Phase 1, often called as the glassy state, during which the storage modulus declines marginally with the increase of temperature due to the stretch of secondary bonds, and some secondary bonds will break. It refers to the temperature range of 0 –72.6℃ for this film adhesive. Phase 2, referred to as the glass transition, during which the storage modulus drops dramatically due to the large-scale breakage of the secondary bonds. It is the temperature range of 72.6 –100℃ for the film adhesive. During phase 3, also named the rubber state, the storage modulus declines to a very low level and almost remains constant thereafter, and it occurs when the temperature exceeds 100℃ for the film adhesive.

There are two common methods for defining the GTT. The first method defines the temperature at the intersection point of the two tangent lines of storage modulus curve as the GTT, which indicates the onset of degradation of storage modulus and is denoted as $T_{g,o}$ [45,46]. Alternatively, the temperature at the maximum loss factor is often defined as the GTT, and it is denoted as $T_{g,t}$ [45,47,48]. As shown in Fig. 5, $T_{g,o}$ and $T_{g,t}$ of the film adhesive J -69E are respectively 71.7℃ and 88.5℃, at which the loss factors are 0.27 and 0.58, respectively.

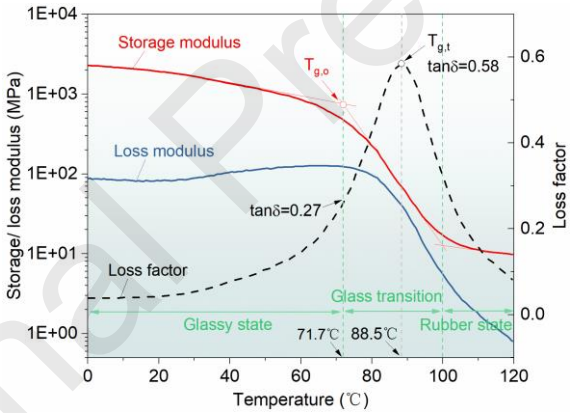


**Fig. 5 DMA results of film adhesive: storage modulus, loss modulus and loss factor versus temperatures.**

### 3.1.2. Comparisons of dynamic mechanical behavior of film adhesive and paste adhesives

In previous studies, the GTTs of most room temperature-cured paste epoxy adhesives are between 40℃ and 70℃, and those of many paste adhesives are even less than 50℃ [8,36,43,45,49,50]. In order to compare the dynamic mechanical behaviors of the film adhesive with the traditional paste epoxy adhesives, the DMA tests for four commonly used paste adhesives were also performed. These paste adhesives include Araldite 2014, Araldite 420, J-133 (typical adhesive used in automobile and aerospace industry in China), and Sika 30. Moreover, the data of dynamic mechanical behaviors of other nine types of paste epoxy adhesive have also been extracted from existing studies. The DMA test set-ups of ten types of epoxy adhesives (numbered from A to J) are tabulated in Table 3. Among these samples, adhesives A, F, and G were cured at medium-high (90℃) or high (120℃) temperatures, while the others were cured at the ambient temperatures (20℃ or 25℃).

**Table 3 DMA test set-ups of various epoxy adhesives.**

| Number | Adhesive type | Curing procedure | Heating rate (℃/min) | Frequency (Hz) | Reference |
|---|---|---|---|---|---|
| A | J -69E | 90℃/2h | 2 | 1 | this paper |
| B | Araldite 2014 | 25℃/7d | 2 | 1 | this paper |
| C | Araldite 420 | 25℃/8d | 2 | 1 | this paper |
| D | J -133 | 25℃/9d | 2 | 1 | this paper |
| E | Sika 30 | 25℃/10d | 2 | 1 | this paper |
| F | S&P resin 220 | 25℃/3d+90℃/25min | 2 | 1 | Michels [45] |
| G | Araldite 2011 | 25℃/2d+120℃/4h | 2 | 1 | Korayem [36] |
| H | Adhesive B | 20℃/7d | 2 | 1 | Custódio [49] |
| I | Adhesive C | 20℃/7d | 2 | 1 | Custódio [49] |
| J | Adhesive D | 20℃/7d | 2 | 1 | Custódio [49] |

The comparisons of the temperature-dependency of mechanical behavior, including the storage modulus, loss factor, and GTT, for the various epoxy adhesives are presented in Fig. 6. The results show that the temperature-dependency of mechanical behavior varied significantly for different epoxy adhesives. As demonstrated in Fig. 6(a), the glass transition segments locate at different temperature ranges for different adhesives. The storage moduli at an identical temperature also varied much with the adhesive types. Specifically, the storage moduli of adhesives E, F, I, and J at the room temperature are extremely larger than those of the others. In Fig. 6(b), a relatively large temperature at the peak and a broadening of loss factor curve were observed for adhesives A, B, F, and G. Among these adhesive samples, adhesives A, F, and G had experienced high-temperature curing, with only adhesive B being an exception which is designed for high-temperature application in the case of being cured at the room temperature. It indicates that suitable high-temperature curing probably enhances the cross-linking density within the epoxy and thus increases the value of GTT, which has been confirmed in related researches [45,49].

As shown in Fig. 6(c), the adhesives A, B, F, and G also have a relatively high value of $T_{g,t}$. However, all these adhesives do not surely possess a high $T_{g,o}$, e.g., the $T_{g,o}$ values of adhesives F and G are relatively low. It will be safer if $T_{g,t}$ was chosen as an index for the evaluation because it denotes the onset of mechanical degradation during temperature increase. Compared with the traditional paste adhesives, the film adhesive possesses higher GTTs and will behave more effectively at elevated temperatures, regardless of which definition methods they are based on. It indicates that, other than the contribution of high-temperature curing effect, the superior high-temperature properties of the film adhesive may also benefit from the enhancing effect of epoxy network crosslinking by the engineering plastic and core-shell structured nanoparticles. The enhancing effect of nanoparticles on the high-temperature behavior of epoxy composites has been verified in previous work [51,52].

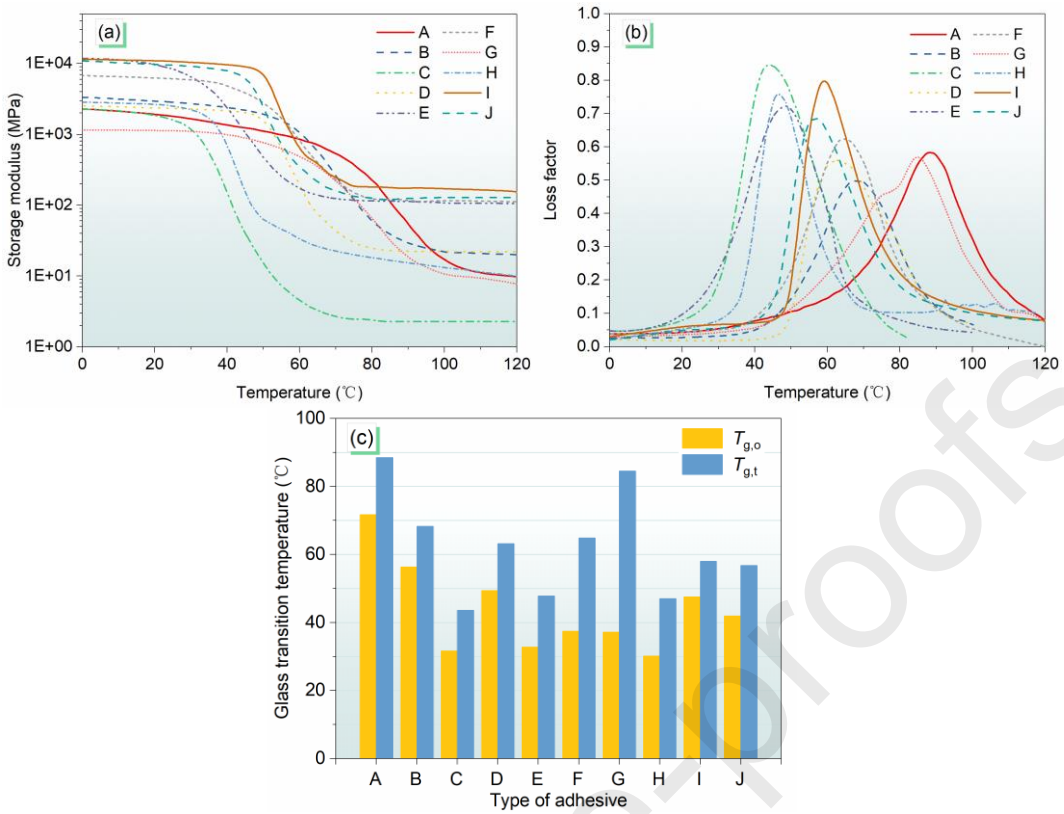


**Fig. 6 Comparisons of the temperature-dependency of mechanical behavior for various epoxy adhesives: (a) storage modulus, (b) loss factor, (c) glass transition temperature.**

### 3.2. Failure modes of bonded joints

The results of the tensile-shear tests for the DLJ specimens are summarized in Table 4. In the table, $D_{\max}$ represents the limit displacement denoting the distance between the loaded end (point A1 in Fig. 3) and fixed end (point B1) when the specimens fails. $P_u$ denotes the ultimate load, and COV denotes the coefficient of variation. $\overline{P}$ is the average bonding strength, as calculated by

$$\overline{f} = \frac{P_u}{L_b \cdot b_f} \tag{1}$$

where $L_b$ and $b_f$ are the bond length and width (i.e. the width of CFRP), respectively.

**Table 4 Results of the tensile-shear tests for DLJ specimens.**

| Series | Specimen tags | Limit displacement (mm) | | | Ultimate load (kN) | | | Average bonding strength (MPa) | | Failure mode |
|---|---|---|---|---|---|---|---|---|---|---|
| | | $D_{\max}$ | Average | COV | $P_u$ | Average | COV | $\overline{f}$ | Average | |
| I | JM-50-1 | 1.93 | 1.95 | 0.030 | 117.2 | 119.3 | 0.034 | 23.44 | 23.85 | d |
| | JM-50-2 | 2.03 | | | 125.0 | | | 25.55 | | d |
| | JM-50-3 | 1.89 | | | 115.6 | | | 23.12 | | d + a |
| II | JM-80-1 | 2.80 | 2.66 | 0.053 | 148.3 | 151.0 | 0.025 | 18.54 | 18.87 | d + a |
| | JM-80-2 | 2.72 | | | 156.4 | | | 19.55 | | d + a |
| | JM-80-3 | 2.47 | | | 148.2 | | | 18.53 | | d + a |
| III | JM-120-1 | 2.51 | 2.48 | 0.010 | 150.4 | 149.2 | 0.017 | 12.53 | 12.44 | d + a |
| | JM-120-2 | 2.45 | | | 145.8 | | | 12.15 | | a + d |

| | | | | | | | | | | |
|---|---|---|---|---|---|---|---|---|---|---|
| | JM-120-3 | 2.49 | | | 151.5 | | | 12.63 | | d + a |
| | JM-160-1 | 2.45 | | | 148.7 | | | 9.29 | | a |
| Ⅳ | JM-160-2 | 2.32 | 2.40 | 0.023 | 145.2 | 147.4 | 0.011 | 9.08 | 9.22 | d + b |
| | JM-160-3 | 2.42 | | | 148.4 | | | 9.28 | | d + a |
| | JM-200-1 | 3.31 | | | 167.0 | | | 8.35 | | d + a |
| Ⅴ | JM-200-2 | 2.73 | 2.79 | 0.146 | 161.3 | 158.4 | 0.054 | 8.07 | 7.92 | d + a |
| | JM-200-3 | 2.32 | | | 146.8 | | | 7.34 | | d |

Notes: Failure mode: a = CFRP-adhesive interface debonding; b = steel-adhesive interface debonding; d = CFRP delamination. Only two major failure modes are listed, and the failure mode before "+" is the predominant one.

The failure modes of all specimens are listed in Table 4 and illustrated in Fig. 7. It is found from the failure photographs that the CFRP delamination (mode d) is the predominant failure mode for most of the specimens. For the specimens with bond lengths of 120 mm and 160 mm, some specimens failed with a distinct mixed mode of CFRP lamination and CFRP-adhesive interface debonding. Among these specimens, one specimen (JM-160-1) failed in CFRP-adhesive interface debonding, which may be caused by the incomplete removal of release agent on the surface of CFRP lamina. Another specimen (JM-160-2) has a small area of a steel-adhesive interface debonding failure, which probably results from fabrication imperfections within the bond line related to incomplete removal of dirt on the steel plates. The predominantly occurred CFRP delamination failure indicates that the bond strengths of the film adhesive with both CFRP and steel are higher than the intra-laminar strength of CFRPs (i.e. the debonding strength of carbon fibers from the resin matrix within CFRP laminas). It also can be implied that the bond strength of the bonded joints probably can be further improved by increasing the intra-laminar strength of CFRP laminas.

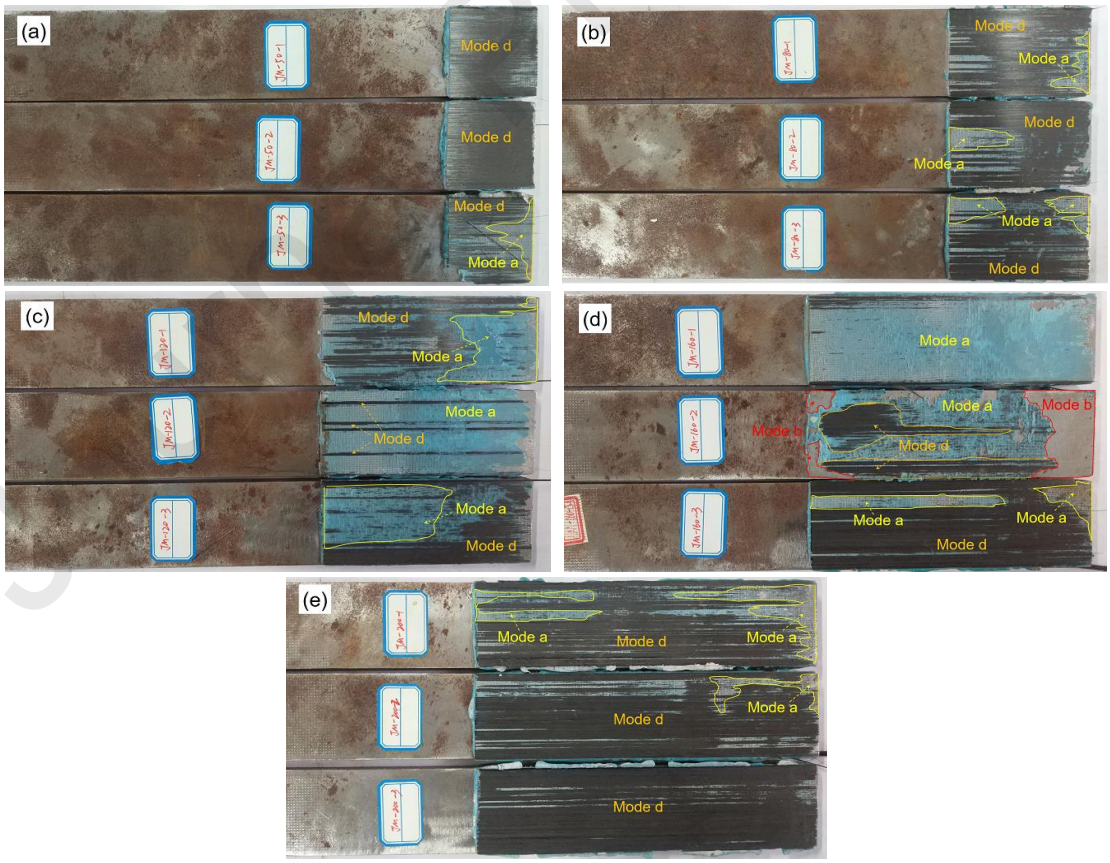


**Fig. 7 Failure modes of the bonded joints: (a) Series Ⅰ: $L_b$ = 50 mm, (b) Series Ⅱ: $L_b$ = 80 mm, (c) Series Ⅲ: $L_b$ = 120 mm, (d) Series Ⅳ: $L_b$ = 160 mm, (e) Series Ⅴ: $L_b$ = 200 mm.**

The micrographs of the fracture surface on the adhesive layer for CFRP delamination were obtained by ZEISS EVO MA25 scanning electron microscope (SEM), as shown in Fig. 8. The results show that large amounts of carbon fibers have remained on the surface of the adhesive layer. It is noted that obvious dimples (pointed out by red arrows) had been produced on the failure interface at the nylon thread intersections of the nylon-fabric carrier, and fiber breakages (pointed out by a yellow box) were observed around these dimples. As carbon fiber break leads to more energy release than the continuous debonding of carbon fibers from epoxy resins, it can be concluded that the nylon thread intersections within the fabric carrier contribute to a better mechanical interlock between the CFRP lamina and adhesive layer.

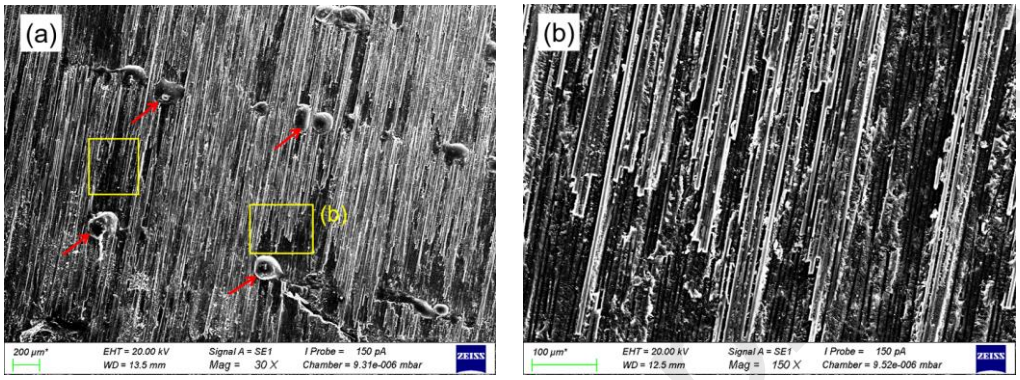


**Fig. 8 SEM images of the fracture surface on adhesive layer: (a) 30 ×, (b) magnification of the fiber breakage, 150 ×.**

### 3.3. Load-displacement response

Fig. 9 depicts the load-displacement relationships during loading for all the specimens tested. The displacement on the x-coordinate axis represents the distance between point A1 and point B1 presented in Fig. 3. As clearly shown in the figures, the load increased linearly with the displacement during the early stage of loading. However, in the later stage of loading, the load-displacement relationships were no longer in linear relation and the slopes of the curves gradually declined. It is because the plastic damage deformation had formed within the bonding layer. This phenomenon indicates that the adhesive film DLJ specimens exhibited a certain ductility in the later stage. At the failure stage, the loads almost directly drop to zero, which indicates a relatively quick failure process.

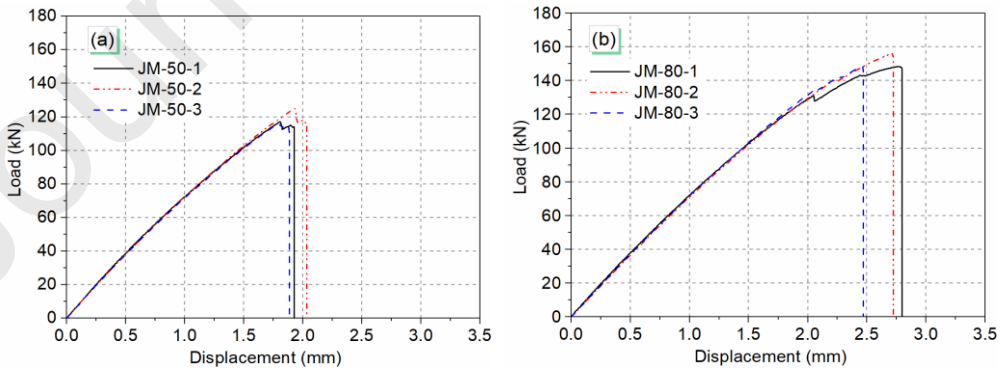

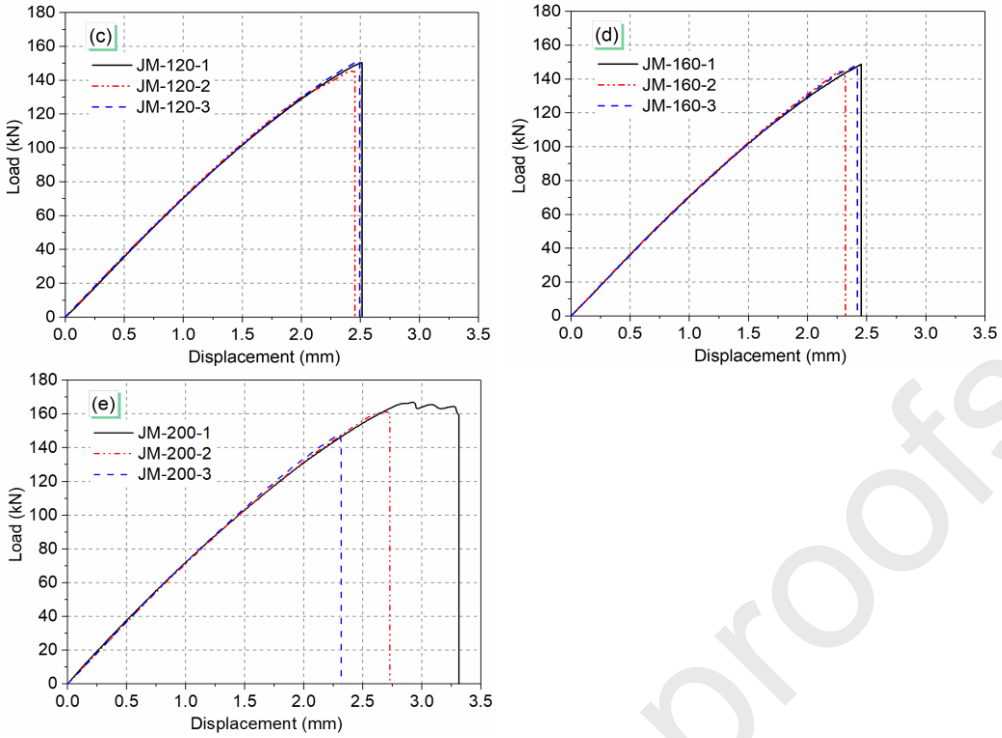


**Fig. 9 Load-displacement relationships and ultimate loads versus bond lengths: (a) Series Ⅰ: $L_b$ = 50 mm, (b) Series Ⅱ: $L_b$ = 80 mm, (c) Series Ⅲ: $L_b$ = 120 mm, (d) Series Ⅳ: $L_b$ = 160 mm, (e) Series Ⅴ: $L_b$ = 200 mm.**

Fig. 10 shows the ultimate load as a function of bond length for the DLJ specimens. It should be noted that it is absolutely true that the ultimate load is zero when the bond length is zero. Moreover, the ultimate load increases linearly as the bond length increases when the joints have an insufficient bond length, as recorded in previous studies [23,43]. The results show that the ultimate load increases with the enhancement of bond length when the bond length is less than 65 mm. However, no significant increase in the ultimate load was observed as the bond length increases when the bond length exceeds 65 mm which is defined as the effective bond length ($L_e$) [53,54]. The appearance of effective bond length is due to the fact that the ultimate load of joints is governed by the concentrated shear stress at the ends of the adhesive layer, but the increase of bond length has little effect on the shear stress concentration once the bond length approaches or exceeds the effective bond length [43]. That is, the effective bond length of the film-adhesive bonding interface is approximately 65 mm at the room temperature. The ultimate bearing capacity of the film adhesive DLJ specimens with sufficient bond lengths is approximately 151.5 kN, i.e., the ultimate load of a single bonding interface is about 75.75 kN.

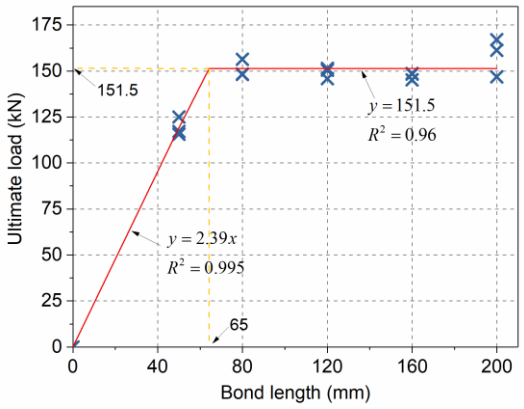


**Fig. 10 Ultimate load as a function of bond length for the DLJs.**

### 3.4. Strain distribution on CFRP lamina

Fig. 11 illustrates the strain distributions on the surfaces of CFRP during loading, with one representative specimen in each series. In the figure, the x-coordinate denotes the distance of the strain gauge away from the loaded end along the bond length direction. The results show that the maximum strain on the surface of CFRP is about 5785 με for Series Ⅰ specimens ($L_b$ =50 mm), while that on the surface of CFRP is 6049–7430 με for Series Ⅱ–Ⅴ specimens ($L_b \geq$ 80 mm). It is implied that the maximum CFRP strain of specimens with a sufficient bond length is higher than that of specimens with an insufficient bond length. At the initial stage of loading, strains are only produced on the CFRPs in the vicinity of the loaded end. With the increase of load, the strains gradually transfer toward the free end, and the strains close to the loaded end increase more quickly than those far away from the loaded end. At the end of loading, the CFRP strains of Series Ⅰ–Ⅱ specimens are approximately distributed in a linear manner along the length direction, while those of Series Ⅲ–Ⅴ specimens are distributed in an exponential manner on the whole. It can be clearly seen from Fig. 11(c)–(e) that the strain gradience is rather steep within the range 75 mm away from the loaded end. However, if the distance exceeds 75 mm, the strains are almost uniformly distributed along the length direction except for the last measuring point, moreover, the strain values increase extremely slow with the increase of load. Since there was no strain gauge arranged between 60 mm and 75 mm and no strains were captured in this region, it can be concluded that the distance of CFRP strain transfer is approximately 60–75 mm which is consistent with the effective bond length obtained from Fig. 10.

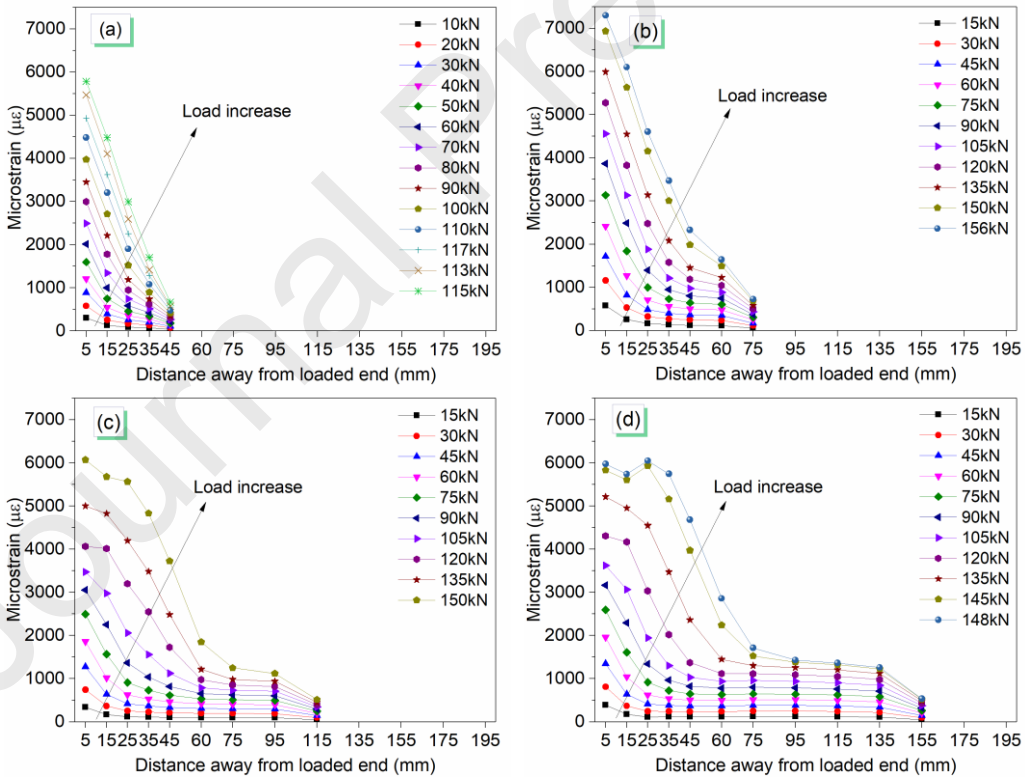

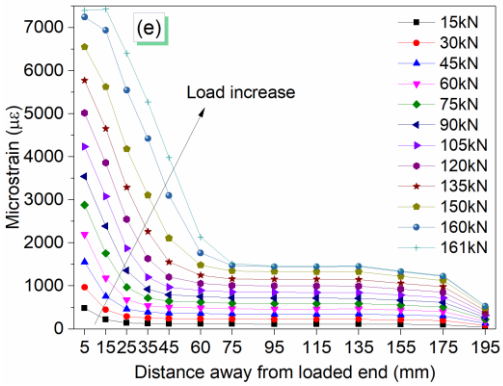


**Fig. 11 Strain distributions on the surfaces of CFRP during loading: (a) Series Ⅰ: $L_b$ = 50 mm, (b) Series Ⅱ: $L_b$ = 80 mm, (c) Series Ⅲ: $L_b$ = 120 mm, (d) Series Ⅳ: $L_b$ = 160 mm, (e) Series Ⅴ: $L_b$ = 200 mm.**

### 3.5. Bond stress distribution within bonding interface

Given that the CFRP lamina is extremely thin compared with the steel plate, it's reasonable to assume a uniform stress distribution along the direction of CFRP's thickness. Therefore, the bond (shear) stresses in the adhesive layer can be calculated from the readings of the strain on the surfaces of CFRP based on a differential equation for the CFRP [11,16,30,54]. The bond stress $\tau_i$ within the bonding interface at the midpoint between the measuring point $i$-1 and $i$ can be expressed by

$$\tau_i = \frac{\Delta\varepsilon_i E_p t_p}{\Delta l_i} = \frac{(\varepsilon_i - \varepsilon_{i-1}) E_p t_p}{l_i - l_{i-1}} \quad (2)$$

where $E_p$ and $t_p$ are the elastic modulus and thickness of CFRP, respectively. $\varepsilon_i$ denotes the strain on the surface of CFRP at the point $i$, and $l_i$ is the distance between the point $i$ and the loaded end. $\Delta\varepsilon_i$ and $\Delta l_i$ are the strain difference and the distance between the point $i$–1 and $i$, respectively.

Fig. 12 depicts the bond stress distributions within the bonding interface along the direction of bond length at different loading stages. The results show that the maximum bond stress locates at the loaded end at the initial stage of loading. However, in the later stage, the maximum bond stress gradually moves toward the position a certain distance away from the loaded end. Prior to the specimen failure, the maximum bond stress locates at the position about 20 mm away from the loaded end for Series Ⅰ–Ⅱ specimens, but it locates 50 mm away from the loaded end for Series Ⅲ–Ⅴ. Thus, one interesting finding can be drawn that the maximum bond stress can transfer farther within joints with a sufficient bond length which seems to be somewhat longer than the effective bond length. Throughout the loading, the bond stresses exceeding 85 mm almost remain zero for Series Ⅲ–Ⅴ specimens, with the stress at the free end as an exception which is caused by the stress concentration. Therefore, the effective transferring distance of the bond stress is 68–85 mm, which is roughly consistent with the effective bond length 65 mm.

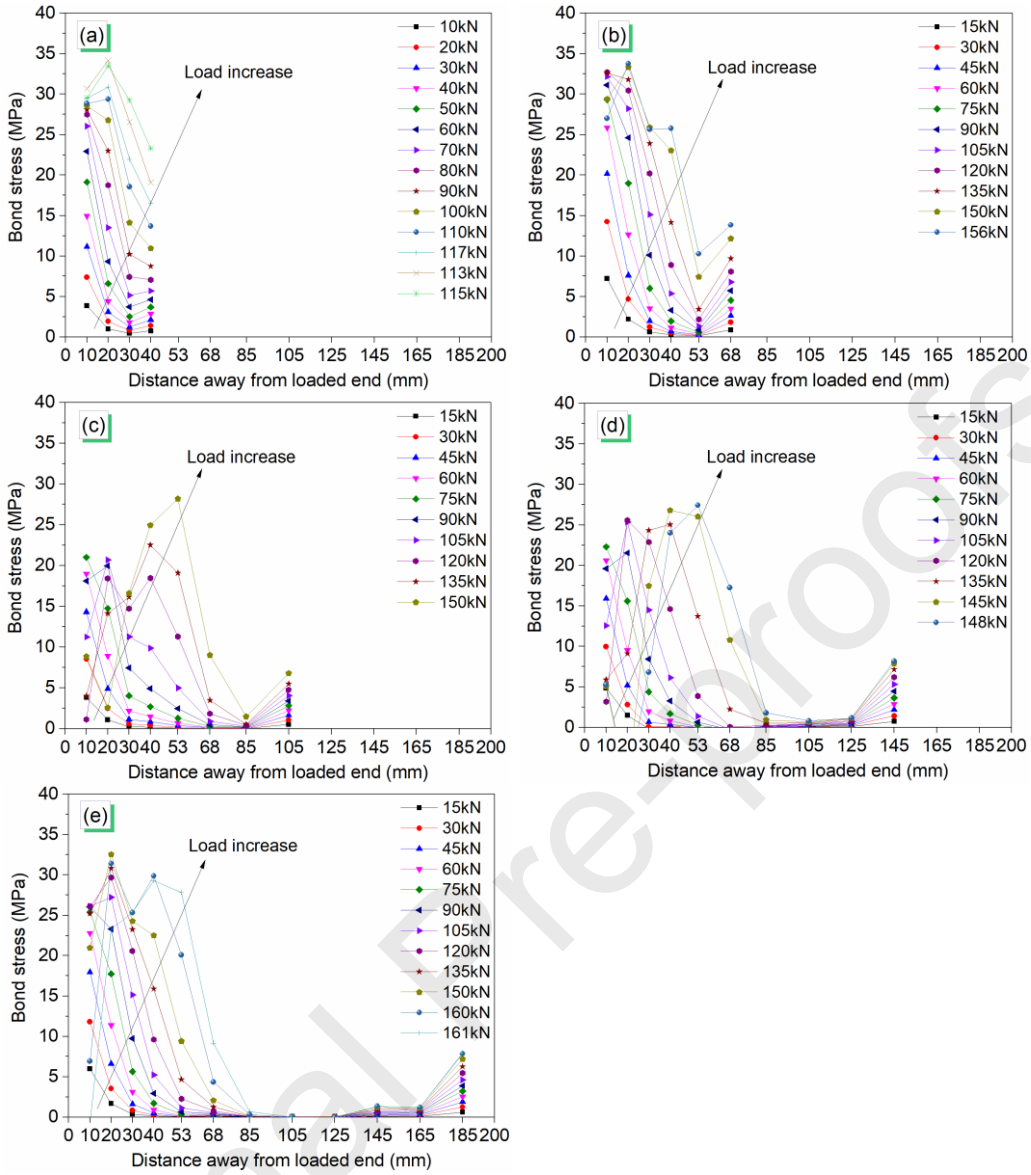


**Fig. 12 Bond stress distributions along the bond length direction: (a) Series Ⅰ: $L_b$ = 50 mm, (b) Series Ⅱ: $L_b$ = 80 mm, (c) Series Ⅲ: $L_b$ = 120 mm, (d) Series Ⅳ: $L_b$ = 160 mm, (e) Series Ⅴ: $L_b$ = 200 mm.**

## 4. Discussion

### 4.1. Bond-slip relationships of film-adhesive bonding interface

The bond behavior of interfaces can be described by the so-called bond-slip relationship (model). The bond-slip relationship depicts the local bond stress ($\tau$) within the bonding interface as a function of the relative slip ($s$) between CFRP and steel and is important for the analytical and numerical modeling of bond behavior. The trapezoidal (trilinear) bond-slip model has been observed in several researches on CFRP/steel composites [12,24,30,55]. This bond-slip curve involves three stages, i.e. ascending branch, plateau branch, and descending (softening) branch, as shown in Fig. 13. Correspondingly, four distinct stages are observed in this model: (1) the elastic stage –the bond stress increases linearly with increasing relative slip, and it is related to the linear stage of the load-displacement curves; (2) the plastic stage –corresponding to the plateau segment during which bond stress remains constant with the increase of local slip; (3) the softening stage –the bond stress starts to decrease as the slip increases; and (4) the debonding stage –the local

interfacial debonding occurs as the bond stress declines to zero. Consequently, the trapezoidal bond-slip model can be generally described with the four parameters including the maximum (peak) bond stress ($\tau_f$), the maximum elastic slip ($s_1$), the maximum plastic slip ($s_2$), and the ultimate slip ($s_f$). The trapezoidal bond-slip model can be expressed as follows:

$$\tau = \begin{cases} \tau_f \cdot \dfrac{s}{s_1} & s \le s_1 \\ \tau_f & s_1 < s \le s_2 \\ \tau_f \cdot \dfrac{s_f - s}{s_f - s_2} & s_2 < s \le s_f \\ 0 & s > s_f \end{cases} \quad (3)$$

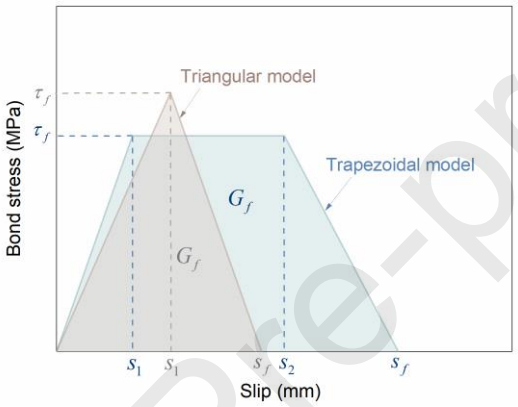


**Fig. 13 Simplified trapezoidal and triangular bond-slip models.**

In this model, the slope of the ascending branch is defined as the initial interfacial stiffness ($K$), as expressed by

$$K = \frac{\tau_f}{s_1} \quad (4)$$

The area underneath the bond-slip curve is often defined as the interfacial fracture energy ($G_f$) which is an important index and is generally applied to characterize the bond strength in analytical and numerical models [13,16,20,24,56]. The interfacial fracture energy can be roughly calculated by

$$G_f = \frac{s_2 - s_1 + s_f}{2} \cdot \tau_f \quad (5)$$

Triangular (bilinear) model is another bond-slip model frequently observed in previous studies [20,26]. This model does not contain a plateau segment in the bond stress-slip curves, thus the parameter $s_2$ (the maximum plastic slip) was removed and composes a triangular curve, as illustrated in Fig. 13. The bilinear bond-slip model can be expressed as

$$\tau = \begin{cases} \tau_f \cdot \dfrac{s}{s_1} & s \le s_1 \\ \tau_f \cdot \dfrac{s_f - s}{s_f - s_1} & s_1 < s \le s_f \\ 0 & s > s_f \end{cases} \quad \textbf{(6)}$$

In the triangular model, the interfacial fracture energy ( $G_f$ ) is roughly calculated by

$$G_f = \frac{s_f \cdot \tau_f}{2} \quad \textbf{(7)}$$

In reference to existing researches, the relative slip between the CFRP and steel can be obtained through numerical integration of the CFRP strain along the bonded length [17,31]. The steel plate deformation can be neglected since the stiffness of the steel plate is of a greater order of magnitude compared with the CFRP. The relative slip $s_{\mathrm{i}}$ at the midpoint between the measuring point $i$ -1 and $i$ can be expressed as

$$s_{\mathrm{i}} = \sum_{j=1}^{i} \frac{\varepsilon_{\mathrm{j}} + \varepsilon_{\mathrm{j\text{-}1}}}{2} \Delta l_{\mathrm{j}} \quad \textbf{(8)}$$

The bond-slip relationships for all the DLJ specimens can be obtained by the combination of Eq. (2) and Eq. (8), as depicted in Fig. 14. For the simplicity of application, the data in this figure were linearly fitted, thus typical trapezoidal bond-slip curves were obtained. The bond-slip curves have ascending and descending branches, as well as a plateau segment between them. The shape of the bond-slip curves obtained here has a good agreement with He et al' researches [30], which also studied the mechanisms of CFRP delamination in CFRP/steel joints. An interesting finding was that the bond-slip relationship for bond length much larger than the effective bond length 65 mm (referred to as "sufficient bond length") is obviously different from that for bond length less than or approaching the effective bond length (referred to as "insufficient bond length"). Concretely, the maximum bond stress and interfacial initial stiffness of the joints with insufficient bond lengths (Series Ⅰ & Ⅱ) are larger than those of the joints with sufficient bond lengths (Series Ⅲ–Ⅴ). However, the maximum elastic slip, maximum plastic slip, and ultimate slip of the joints with insufficient bond lengths are smaller than those of the joints with sufficient bond lengths. Another noteworthy finding is that the descending branches in the bond-slip curves of the joints with insufficient bond lengths developed imperfectly. On the contrary, the descending branches for the joints with sufficient bond lengths developed fully and almost extended to bond stress zero. Similar phenomena have also been observed in the studies of Biscaia et al. [31].

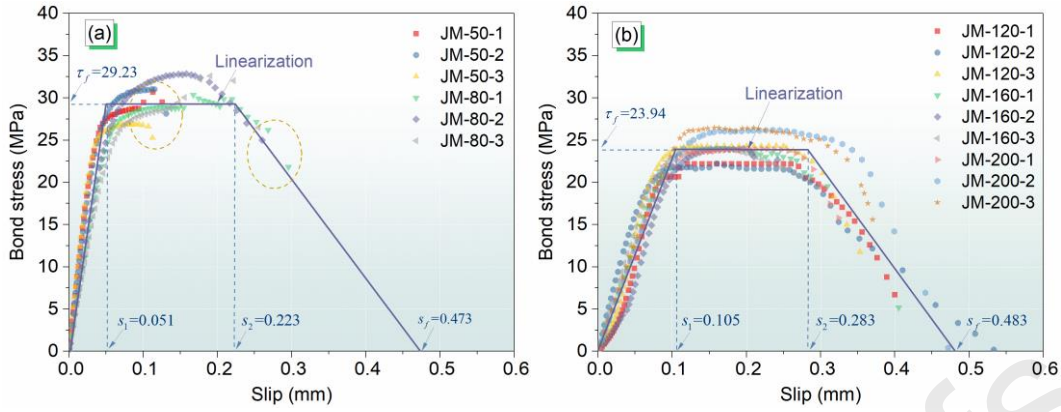


**Fig. 14 Bond-slip relationships for the film-adhesive bonding interface: (a) Series Ⅰ & Ⅱ; (b) Series Ⅲ–Ⅴ.**

## 4.2. Comparisons of bond-slip relationships of film-adhesive and paste-adhesive bonding interfaces

In order to have extensive insight into the bond-slip behavior of CFRP/steel bonded joints with sufficient bond lengths, a database was built based on these tests and previous studies. All the data collected are from specimens with a sufficient bond length and with an adhesive thickness of approximately 1.0 mm. The specimen details and test results of 26 paste-adhesive joints from the previous studies are summarized in Table 5. In the table, each type of bonding interface has been numbered with a lower-case letter.

**Table 5 Specimen details and test results.**

| Adhesive type | Number | Specimen tags | Test method | $L_b$ (mm) | $t_a$ (mm) | Adhesive | | CFRP plate | | | $P_u$ (kN) | failure mode | Reference |
|---|---|---|---|---|---|---|---|---|---|---|---|---|---|
| | | | | | | Adhesive | $\sigma_{max}$ (MPa) | $E_a$ (GPa) | $b_f$ (mm) | $t_f$ (mm) | $E_f$ (GPa) | | | |
| Nonlinear adhesives | b | Tc-1 | Pull-push, single shear | 180 | 1.00 | Tc | 25.7 | 1.50 | 25 | 1.44 | 185 | 62.39 | d | He [30] |
| | | Tc-2 | | 180 | 1.00 | Tc | 25.7 | 1.50 | 25 | 1.44 | 185 | 64.95 | d | |
| | | Tc-3 | | 180 | 1.00 | Tc | 25.7 | 1.50 | 25 | 1.44 | 185 | 60.74 | d | |
| | | Tc-4 | | 180 | 1.00 | Tc | 25.7 | 1.50 | 25 | 1.44 | 185 | 63.94 | d | |
| | c | A350-1.0-1 | Pull-push, single shear | 350 | 0.99 | Araldite 2015 | 15.1 | 1.75 | 50 | 1.4 | 165 | 108.5 | c | Wang [28] |
| | | A350-1.0-2 | | 350 | 1.05 | Araldite 2015 | 15.1 | 1.75 | 50 | 1.4 | 165 | 109.2 | c | |
| | d | C-NM-T1-Ⅰ | | 300 | 0.99 | Araldite 2015 | 14.73 | 1.75 | 50 | 1.2 | 150 | 112.87 | c | |
| | | C-NM-T1-Ⅱ | | 300 | 1.02 | Araldite 2015 | 14.73 | 1.75 | 50 | 1.2 | 150 | 113.81 | c | |
| Linear adhesives | e | F1.4-A1.0-1 | Pull-pull, single shear | 180 | 1.17 | Araldite 420 | 30.5 | 2.41 | 50 | 1.4 | 161.2 | 84 | a + d | Li [20] |
| | | F1.4-A1.0-2 | | 180 | 1.12 | Araldite 420 | 30.5 | 2.41 | 50 | 1.4 | 161.2 | 78 | a + d | |
| | | F1.4-A1.0-3 | | 180 | 1.18 | Araldite 420 | 30.5 | 2.41 | 50 | 1.4 | 161.2 | 84 | a + d | |
| | f | F1.4-L1-1 | | 180 | 1.14 | Lica 131 | 26.6 | 3.99 | 50 | 1.4 | 161.2 | 51 | a + b | Li [20] |
| | | F1.4-L1-2 | | 180 | 1.09 | Lica 131 | 26.6 | 3.99 | 50 | 1.4 | 161.2 | 46 | a + b | |
| | | F1.4-L1-3 | | 180 | 1.03 | Lica 131 | 26.6 | 3.99 | 50 | 1.4 | 161.2 | 44 | a + b | |
| | g | F1.4-S1-1 | | 180 | 1.15 | Sika 330 | 24.4 | 4.87 | 50 | 1.4 | 161.2 | 40 | a + b | |
| | | F1.4-S1-2 | | 180 | 1.12 | Sika 330 | 24.4 | 4.87 | 50 | 1.4 | 161.2 | 41 | a + b | |
| | | F1.4-S1-3 | | 180 | 1.13 | Sika 330 | 24.4 | 4.87 | 50 | 1.4 | 161.2 | 42 | a + b | |

| | | | | | | | | | | | | |
|---|---|---|---|---|---|---|---|---|---|---|---|---|
| | F1.4-S1-4 | | 180 | 1.18 | Sika 330 | 24.4 | 4.87 | 50 | 1.4 | 161.2 | 40 | a + b | |
| | F1.4-S1-5 | | 180 | 1.14 | Sika 330 | 24.4 | 4.87 | 50 | 1.4 | 161.2 | 40 | a + b | |
| | F1.4-s1-1 | | 180 | 1.08 | Sika 30 | 25.3 | 12.13 | 50 | 1.4 | 161.2 | 37 | c | |
| h | F1.4-s1-2 | | 180 | 1.09 | Sika 30 | 25.3 | 12.13 | 50 | 1.4 | 161.2 | 35 | c | |
| | F1.4-s1-3 | | 180 | 1.19 | Sika 30 | 25.3 | 12.13 | 50 | 1.4 | 161.2 | 34 | a + c | |
| i | A-1 | Pull-push, single shear | 350 | 1.07 | A | 22.53 | 4.01 | 50 | 1.2 | 165 | 60.5 | c | Akbar [26] |
| j | B-1 | | 350 | 0.83 | B | 20.48 | 10.79 | 50 | 1.2 | 165 | 39.4 | c | |
| k | A-NM-T1-Ⅰ | Pull-push, single shear | 300 | 1.07 | Sika 30 | 22.34 | 11.25 | 50 | 1.2 | 150 | 30.75 | c | Yu [12] |
| | A-NM-T1-Ⅱ | | 300 | 1.03 | Sika 30 | 22.34 | 11.25 | 50 | 1.2 | 150 | 31.21 | c | |

Notes: 1. $L_b$ = bond length, $t_a$ = thickness of adhesive layer, $\sigma_{\max}$ = tensile strength of adhesive, $E_a$ = elastic modulus of adhesive, $b_f$ = width of CFRP, $t_f$ = thickness of CFRP, $E_f$ = elastic modulus of CFRP, $P_u$ = ultimate load when specimens fail.

2. Failure modes: a = CFRP-adhesive interface debonding; b = steel-adhesive interface debonding; c = cohesive failure; d = CFRP delamination.

In order to have a comparison of the bond-slip behaviors of CFRP/steel bonding interfaces composed of different adhesive materials, the simplified bond-slip curves for different bonding interfaces with a sufficient bond length are plotted in Fig. 15. In this figure, each type of bonding interface has been marked with the lower-case letter, the adhesive type, and the failure mode (in brackets).

As shown in Fig. 15, bonding interface types a–d have a trapezoidal bond-slip relationship, while the others exhibit triangular ones. An interesting finding is that the bonded interfaces composed of different adhesive materials have different failure modes, and the various failure modes are responsible for the different bond-slip relationships. Concretely, the interfacial debonding failures, including modes a and b or their mixed mode, have a triangular bond-slip model and exhibit as a brittle failure manner. In contrast, the cohesive failure and CFRP delamination (i.e. the interfaces a–d) have a trapezoidal bond-slip model, which contains a plateau segment and shows characteristics of interfacial ductility. It should be also noted that although the bonding interfaces h and k failed with cohesive failure (mode c), their bond-slip models are in bilinear shape, it is because the adhesive Sika 30 is a typical linear adhesive with brittle mechanical characteristic [12,20].

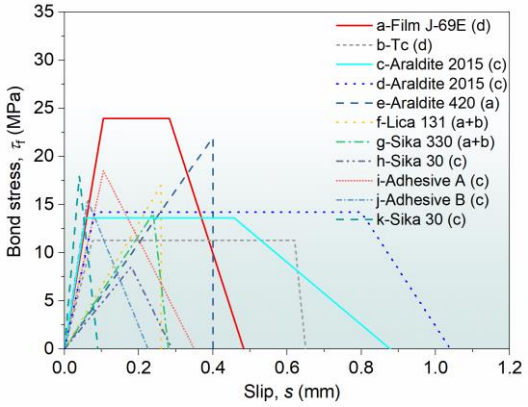


**Fig. 15 Comparison of bond-slip models of different CFRP/steel bonding interfaces.**

Note: Failure modes: a = CFRP–adhesive interface debonding, b = adhesive–steel interface debonding, c = cohesive failure, d = CFRP superficial delamination.

The bond-slip parameters are extracted from Fig. 15 and are compared in Fig. 16. Results in Fig. 16(a) show that the maximum bond stress of film-adhesive bonding interface (interface a) is the largest, indicating that the film adhesive provides the strongest resistance for local debonding induced by concentrated stresses. Results in Fig. 16 (b) demonstrate that the initial interfacial stiffness of the film-adhesive bonding interface is relatively high. It implies that the film-adhesive interface will provide a strong restraint for crack propagation once it is used for crack repair. Fig. 16(c) shows the maximum elastic slips, i.e. the slips at the onset of plastic damages. The maximum elastic slip of the film-adhesive interface is relatively low. Only the interfaces with trapezoidal bond-slip relationships have the index–maximum plastic slip ( $s_2$ ). Fig. 16(d) shows that the maximum plastic slip of the film-adhesive interface is the smallest. As shown in Fig. 16(e)-(f), bonding interfaces with trapezoidal bond-slip models (interfaces a–d) have a large ultimate slip and fracture energy, respectively indicating an excellent mechanical ductility and a massive energy release at debonding.

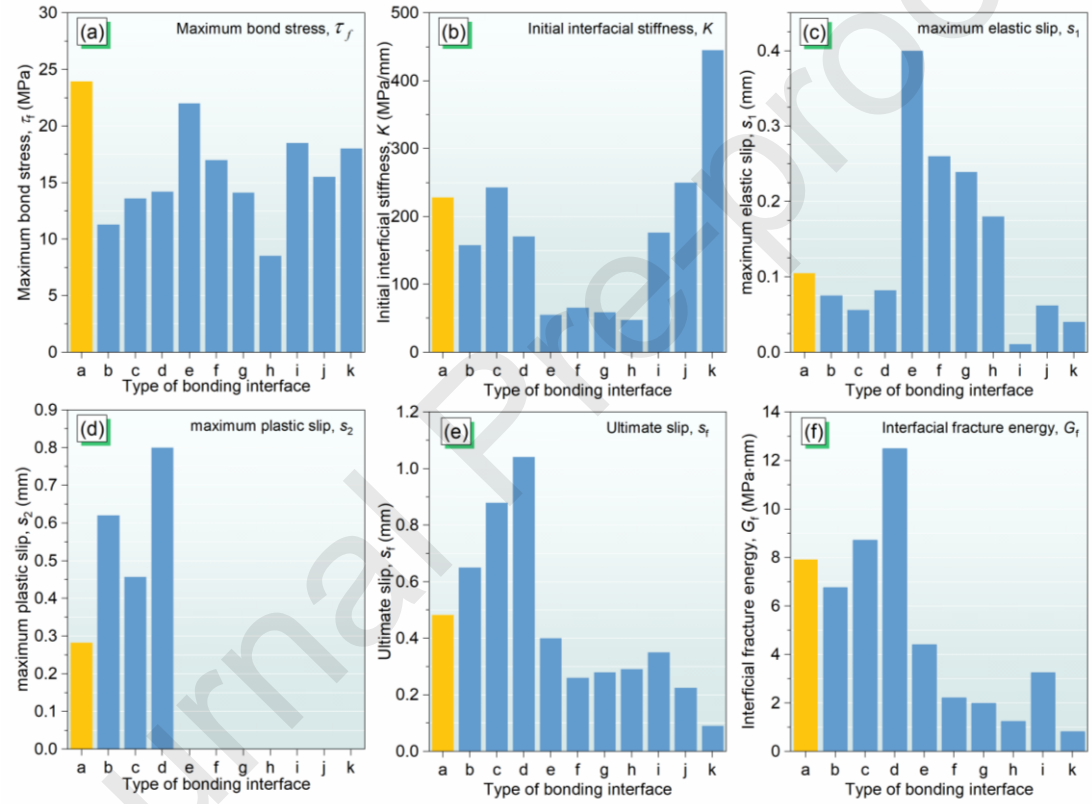


**Fig. 16 Comparisons of bond-slip parameters: (a) maximum bond stress, (b) initial interfacial stiffness, (c) maximum elastic slip, (d) maximum plastic slip, (e) ultimate slip, (f) interfacial fracture energy.**

### 4.3. Comparisons of bond strengths of film-adhesive and paste-adhesive bonding interfaces

Based on the fracture mechanics approach, the ultimate load (bond strength) can be calculated using the interfacial fracture energy for the bonded interfaces with both bilinear and trapezoidal bond-slip models[11,29]. When the bond length ( $L_b$ ) is larger than the effective bond length ( $L_e$ ), the ultimate load ( $P_{u,cal}$ ) can be predicted by

$$P_{u,cal} = b_f \Big/ \sqrt{\frac{1}{2G_f}\left(\frac{1}{E_f t_f} + \frac{b_f}{E_s t_s b_s}\right)} \quad if \quad L_b \geq L_e \tag{9}$$

where $E_s$ , $t_s$ and $b_s$ are the elastic modulus, thickness, and width of the steel plates,

respectively.

Since the axial stiffness of the steel plate is much larger than that of the CFRP, the assumption $b_f / E_s t_s b_s = 0$ can be achieved. Therefore, the above equation can be simplified to the well-known expression which has been studied in many existing studies on CFRP/steel or CFRP-concrete bonding interfaces[11,12,16,28,57]:

$$P_{u,cal} = b_f \sqrt{2 G_f E_f t_f} \tag{10}$$

The ultimate loads of all these specimens are calculated by Eq. (10), and the comparison of predicted and experimental results are plotted in Fig. 17. The results show that, other than the bonding interfaces a and b, theoretical results demonstrate satisfactory agreement with the test results, with a deviation of no more than 16%. An important finding is that the deviation between the theoretical and experimental results for the bonding interfaces a and b (failing with CFRP delamination) is 25%, being the largest among all the samples. Thus, this theoretical model may induce a considerable error when used for predicting the ultimate loads for CFRP delamination. It is because this theory was derived based on the assumption that the failure occurs in the adhesive layer and the properties of both adherents remain constant during the loading. In fact, the ultimate loads of interfaces a and b highly depend on the mechanical properties of CFRP laminas which, however, has been damaged by the fiber tearing. We suggest that a failure criterion of CFRP laminas, e.g., Tsai-Wu criterion [58], should be adopted to achieve a more precise prediction of the ultimate load of bonded joints in the case of CFRP delamination failure.

As shown in Fig. 17(b), almost all bonding interfaces with trapezoidal bond-slip relationships, i.e., interfaces a–d, are of relatively high ultimate bearing capacities. The interface e is an exception, and it has a bilinear bond-slip relationship. However, it still possesses a considerably high ultimate load. The bonding interfaces c–e, (respectively bonded with adhesives Araldite 2015, Araldite 2015, and Araldite 420) have almost equal or better bond strengths to/than that of the bonding interface a (bonded with the film adhesive). However, the high-temperature resistance of these interfaces is lower than the bonding interface a. Concretely, the GTT of Araldite 2015 is about 67℃ when cured at 40℃ for 2–16h, as obtained from differential scanning calorimetry (DSC) tests [59,60]. The $T_{g,o}$ and $T_{g,t}$ of Araldite 420 are respectively 31.6℃ and 43.6℃ as shown in Fig. 6(c). Thus, the GTTs of adhesives Araldite 420 and Araldite 2015 are much lower than the film adhesive ($T_{g,o}$=71.7℃, $T_{g,t}$=88.5℃). By a general consideration of the bond strength, ductility, and high-temperature behavior, the film adhesive shows the best comprehensive performance for bonding CFRP laminas to steel substrates.

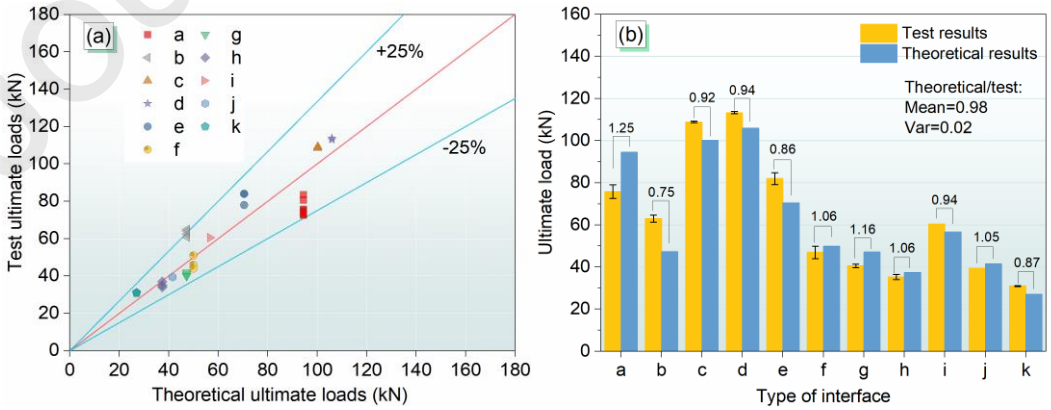


**Fig. 17 (a) Comparisons of test and predicted results of ultimate load for each specimen; (b) comparisons of average values of ultimate load for different types of interface.**

## 5. Conclusions

This paper investigated the bond behavior between CFRP lamina and steel plate with a novel nylon-carrier supported film adhesive. Compared to traditional two-component paste adhesives, the film adhesive possesses many advantageous features such as proper ductility, excellent high-temperature resistance, convenient storage and conveyance, and easy control of adhesive layer thickness during curing process. The high-temperature behavior of the film adhesive was investigated via DMA. CFRP/steel DLJ specimens with different bond lengths were tested under tensile-shear set-up, of which the results including the failure mode, load-displacement response, CFRP strain distribution, and bond stress distribution were presented. Then, the interfacial bond-slip relationships for the film-adhesive bonding interface were established and compared with traditional paste-adhesive bonding interfaces. Finally, the existing bond strength model was validated with the experimental results and the collected data. The following conclusions are drawn:

- The innovative film adhesive is of excellent high-temperature mechanical resistance. The film adhesive possesses the highest GTT compared with frequently used paste adhesives as shown by the DMA results, regardless of which definitions to be based on.
- The film adhesive DLJ specimens mainly failed in the mode of CFRP delamination. It indicates that the film adhesive provides a stronger bond with both the CFRP and steel than the intra-laminar strength of CFRP laminas. The SEM images of the joint fracture interfaces reveal that the nylon-fabric carrier within the film adhesive contributes to a stronger mechanical interlock between the CFRP and adhesive layer.
- The film-adhesive CFRP/steel bonded joints have an effective bond length of approximately 65 mm, beyond which no increase of ultimate bearing capacity can be achieved with the increase of bond length.
- The film-adhesive bonding interface has a trapezoidal bond-slip relationship, indicating an appropriate interfacial ductility. This trapezoidal bond-slip relationship is significantly different from the triangular ones for most paste-adhesive bonding interfaces whose failure shows brittle.
- The maximum bond stress for the film-adhesive bonding interface is the largest; thus this bonding interface has the highest resistance for local debonding induced by concentrated stress. Moreover, the film-adhesive bond line has a relatively high initial interfacial stiffness and thus is supposed to form a stronger restraint for the crack once it is used for crack repair.
- Compared with traditional paste-adhesive bonding interfaces, the film-adhesive bonding interface possesses not only excellent bond strength but also reasonably superior ductility. Moreover, this bonding interface is supposed to have a proper high-temperature resistance via the DMA results of the film adhesive.

## Declaration of Conflict of interest

None.

## Acknowledgments

The authors gratefully acknowledge the financial support from the National Natural Science Foundation of China [Grant Nos. 51778069 & 51708047], the China Scholarship Council [Grant No. 201808430209], the National Program on Key Basic Research Project of China (973 Program) [Grant No. 2015CB057701], and the Horizon 2020- Marie Skłodowska-Curie Individual Fellowship of European Commission [Grant No. 793787].

## Data availability

The raw/processed data required to reproduce these findings cannot be shared at this time due to technical or time limitations.

## References:


[1] Zhao X, Bai Y, Al-Mahaidi R, Rizkalla S. Effect of dynamic loading and environmental conditions on the bond between cfrp and steel: State-of-the-art review. J. Compos Constr 2014;18(3).

[2] Teng JG, Yu T, Fernando D. Strengthening of steel structures with fiber-reinforced polymer composites. J. Constr Steel Res 2012;78:131-43.

[3] Zhou Y, Chen X, Fan Z, Sui L, Li D, Xing F. Bond behaviors of FRP-to-concrete interface under the control of a novel end-anchorage system. Compos Struct 2017;168:130-42.

[4] Dong K, Hu K. Development of bond strength model for CFRP-to-concrete joints at high temperatures. Composites Part B: Engineering 2016;95:264-71.

[5] Sen R. Developments in the durability of FRP-concrete bond. Constr Build Mater 2015;78:112-25.

[6] Firmo JP, Correia JR, Bisby LA. Fire behaviour of FRP-strengthened reinforced concrete structural elements: A state-of-the-art review. Composites Part B 2015;80:198-216.

[7] Heshmati M, Haghani R, Al-Emrani M. Environmental durability of adhesively bonded FRP/steel joints in civil engineering applications: State of the art. Composites Part B: Engineering 2015;81:259-75.

[8] Gholami M, Sam ARM, Yatim JM, Tahir MM. A review on steel/CFRP strengthening systems focusing environmental performance. Constr Build Mater 2013;47:301-10.

[9] Yu Q, Gu X, Zhao X, Zhang D, Huang H, Jiang C. Characterization of model uncertainty of adhesively bonded CFRP-to-steel joints. Compos Struct 2019;215:150-65.

[10] Yang Y, Biscaia H, Chastre C, Silva MAG. Bond characteristics of CFRP-to-steel joints. J. Constr Steel Res 2017;138:401-19.

[11] Xia SH, Teng JG.Behaviour of FRP-to-steel bonded joints. Hong Kong, China: International Institute for FRP in Construction (IIFC);2005. p. 411-8.

[12] Yu T, Fernando D, Teng JG, Zhao XL. Experimental study on CFRP-to-steel bonded interfaces. Composites Part B: Engineering 2012;43(5):2279-89.

[13] Tang H, Deng X, Lin Z, Zhou X. Analytical and experimental investigation on bond behavior of CFRP-to-stainless steel interface. Compos Struct 2019;212:94-105.

[14] Mu W, Qin G, Na J, Tan W, Liu H, Luan J. Effect of alternating load on the residual strength of environmentally aged adhesively bonded CFRP-aluminum alloy joints. Composites Part B: Engineering 2019;168:87-97.

[15] Yu Q, Gao R, Gu X, Zhao X, Chen T. Bond behavior of CFRP-steel double-lap joints exposed to marine atmosphere and fatigue loading. Eng Struct 2018;175:76-85.

[16] Ceroni F, Ianniciello M, Pecce M. Bond behavior of FRP carbon plates externally bonded over steel and concrete elements: Experimental outcomes and numerical investigations. Composites Part B: Engineering 2016;92:434-46.

[17] He J, Xian G. Bond-slip behavior of fiber reinforced polymer strips-steel interface. Constr Build Mater 2017;155:250-8.

[18] Al-Mosawe A, Al-Mahaidi R, Zhao X. Effect of CFRP properties, on the bond characteristics

between steel and CFRP laminate under quasi-static loading. Constr Build Mater 2015;98:489-501.

[19] Hart-Smith L J. Adhesive-bonded double-lap joints. NASA contract report, 1973.

[20] Li C, Ke L, He J, Chen Z, Jiao Y. Effects of mechanical properties of adhesive and CFRP on the bond behavior in CFRP-strengthened steel structures. Compos Struct 2019;211:163-74.

[21] Martinelli E, Hosseini A, Ghafoori E, Motavalli M. Behavior of prestressed CFRP plates bonded to steel substrate: Numerical modeling and experimental validation. Compos Struct 2019;207:974-84.

[22] Zhou H, Torres JP, Fernando D, Law A, Emberley R. The bond behaviour of CFRP-to-steel bonded joints with varying bond properties at elevated temperatures. Eng Struct 2019;183:1121-33.

[23] Wu C, Zhao X, Hui Duan W, Al-Mahaidi R. Bond characteristics between ultra high modulus CFRP laminates and steel. Thin Wall Struct 2012;51:147-57.

[24] Wang H, Wu G. Bond-slip models for CFRP plates externally bonded to steel substrates. Compos Struct 2018;184:1204-14.

[25] Fawzia S, Zhao X, Al-Mahaidi R. Bond – slip models for double strap joints strengthened by CFRP. Compos Struct 2010;92(9):2137-45.

[26] Akbar I, Oehlers DJ, Mohamed Ali MS. Derivation of the bond – slip characteristics for FRP plated steel members. J. Constr Steel Res 2010;66(8-9):1047-56.

[27] Teng JG, Fernando D, Yu T, Zhao XL. Treatment of Steel Surfaces for Effective Adhesive Bonding. Berlin, Heidelberg: Springer Berlin Heidelberg;2011. p. 865-8.

[28] Wang H, Wu G, Dai Y, He X. Experimental Study on Bond Behavior between CFRP Plates and Steel Substrates Using Digital Image Correlation. J. Compos Constr 2016;20(6).

[29] Fernando D, Yu T, Teng JG. Behavior of CFRP Laminates Bonded to a Steel Substrate Using a Ductile Adhesive. J. Compos Constr 2014;18(2):4013010-40.

[30] He J, Xian G. Debonding of CFRP-to-steel joints with CFRP delamination. Compos Struct 2016;153:12-20.

[31] Biscaia HC, Chastre C, Borba IS, Silva C, Cruz D. Experimental evaluation of bonding between CFRP laminates and different structural materials. J. Compos Constr 2016;20(3).

[32] Angelidi M, Vassilopoulos AP, Keller T. Displacement rate and structural effects on Poisson ratio of a ductile structural adhesive in tension and compression. Int J. Adhes Adhes 2017;78:13-22.

[33] Jia Z, Yuan G, Feng X, Zou Y, Yu J. Shear properties of polyurethane ductile adhesive at low temperatures under high strain rate conditions. Composites Part B: Engineering 2019;156:292-302.

[34] Stein N, Rosendahl PL, Becker W. Modelling load transfer and mixed-mode fracture of ductile adhesive composite joints. Int J. Adhes Adhes 2018;82:299-310.

[35] Sousa JM, Correia JR, Cabral-Fonseca S. Durability of an epoxy adhesive used in civil structural applications. Constr Build Mater 2018;161:618-33.

[36] Korayem AH, Chen SJ, Zhang QH, Li CY, Zhao XL, Duan WH. Failure of CFRP-to-steel double strap joint bonded using carbon nanotubes modified epoxy adhesive at moderately elevated temperatures. Composites Part B: Engineering 2016;94:95-101.

[37] Qin G, Na J, Mu W, Tan W, Yang J, Ren J. Effect of continuous high temperature exposure on the adhesive strength of epoxy adhesive, CFRP and adhesively bonded CFRP-aluminum alloy joints. Composites Part B: Engineering 2018;154:43-55.

[38] Bai Y, Nguyen TC, Zhao XL, Al-Mahaidi R. Environment-Assisted Degradation of the Bond between Steel and Carbon-Fiber-Reinforced Polymer. J. Mater Civil Eng 2014;26(9):4014054.

[39] ASTM D638-14. Standard Test Method for Tensile Properties of Plastics; 2014.

[40] ASTM D3528-96. Standard Test Method for Strength Properties of Double Lap Shear Adhesive Joints by Tension Loading; 2016.

[41] Al-Mosawe A, Al-Mahaidi R, Zhao X. Bond behaviour between CFRP laminates and steel members under different loading rates. Compos Struct 2016;148:236-51.

[42] Silva MAG, Biscaia H, Ribeiro P. On factors affecting CFRP-steel bonded joints. Constr Build Mater 2019;226:360-75.

[43] Nguyen T, Bai Y, Zhao X, Al-Mahaidi R. Mechanical characterization of steel/CFRP double strap joints at elevated temperatures. Compos Struct 2011;93(6):1604-12.

[44] Moussa O, Vassilopoulos AP, de Castro J, Keller T. Time–temperature dependence of thermomechanical recovery of cold-curing structural adhesives. Int J. Adhes Adhes 2012;35:94-101.

[45] Michels J, Widmann R, Czaderski C, Allahvirdizadeh R, Motavalli M. Glass transition evaluation of commercially available epoxy resins used for civil engineering applications. Composites Part B: Engineering 2015;77:484-93.

[46] Standard Test Method for Assignment of the Glass Transition Temperature By Dynamic Mechanical Analysis1.

[47] Dehghan M, Al-Mahaidi R, Sbarski I, Gad E. Effect of Fabrication Method on Thermo-mechanical Properties of an Epoxy Composite. The Journal of Adhesion 2014;90(5-6):368-83.

[48] Korayem AH, Barati MR, Simon GP, Zhao XL, Duan WH. Reinforcing brittle and ductile epoxy matrices using carbon nanotubes masterbatch. Composites Part A: Applied Science and Manufacturing 2014;61:126-33.

[49] Custódio J, Broughton J, Cruz H. Rehabilitation of timber structures – Preparation and environmental service condition effects on the bulk performance of epoxy adhesives. Constr Build Mater 2011;25(8):3570-82.

[50] Zhang Y, Vassilopoulos AP, Keller T. Effects of low and high temperatures on tensile behavior of adhesively-bonded GFRP joints. Compos Struct 2010;92(7):1631-9.

[51] Rosso P, Ye L. Epoxy/Silica Nanocomposites: Nanoparticle-Induced Cure Kinetics and Microstructure. Macromol Rapid Comm 2007;28(1):121-6.

[52] Zhu J, Wei S, Ryu J, Sun L, Luo Z, Guo Z. Magnetic Epoxy Resin Nanocomposites Reinforced with Core−Shell Structured Fe@FeO Nanoparticles: Fabrication and Property Analysis. Acs Appl. Mater. Inter. 2010;2(7):2100-7.

[53] Fawzia S. Evaluation of shear stress and slip relationship of composite lap joints. Compos Struct 2013;100:548-53.

[54] Al-Zubaidy H, Al-Mahaidi R, Zhao X. Experimental investigation of bond characteristics between CFRP fabrics and steel plate joints under impact tensile loads. Compos Struct 2012;94(2):510-8.

[55] Korayem AH, Li CY, Zhang QH, Zhao XL, Duan WH. Effect of carbon nanotube modified epoxy adhesive on CFRP-to-steel interface. Composites Part B: Engineering 2015;79:95-104.

[56] Haghani R. Analysis of adhesive joints used to bond FRP laminates to steel members – A numerical and experimental study. Constr Build Mater 2010;24(11):2243-51.

[57] Biscaia HC, Chastre C, Silva MAG. Bond-slip model for FRP-to-concrete bonded joints under external compression. Composites Part B: Engineering 2015;80:246-59.

[58] Ye J, Yan Y, Hong Y, Guo F. An integrated constitutive model for tensile failure analysis and overlap design of adhesive-bonded composite joints. Compos Struct 2019;223:110986.

[59] Huntsman Corporation. Advanced Materials Technical Datasheet–Araldite® 2015 Adhesive. Huntsman Corporation; 2015.

[60] Özer H, Erbayrak E. The effects of curing temperature on fracture energy and cohesive parameters for the adhesive Araldite 2015. J. Adhes Sci Technol 2018;32(12):1287-312.